Tantalum Oxide Electron-Selective Heterocontacts for Silicon Photovoltaics and Photoelectrochemical Water Reduction

Yimao Wan[*†1,2,3], *Siva Krishna Karuturi*[†4], *Christian Samundsett*[1], *James Bullock*[2,3], *Mark Hettick*[2,3], *Di Yan*[1], *Jun Peng*[1], *Parvathala Reddy Narangari*[4], *Sudha Mokkapati*[5], *Hark Hoe Tan*[4], *Chennupati Jagadish*[4], *Ali Javey*[2,3], *and Andres Cuevas*[1]

[1] Research School of Engineering, The Australian National University (ANU), Canberra, ACT 0200, Australia

[2] Department of Electrical Engineering and Computer Sciences, University of California, Berkeley, California 94720, USA

[3] Materials Sciences Division, Lawrence Berkeley National Laboratory, Berkeley, California 94720, USA

[4] Department of Electronic Materials Engineering, Australian National University (ANU), Canberra, ACT 0200, Australia

[5] School of Physics and Astronomy, Cardiff University, Cardiff, Wales, UK

*** Corresponding Author** yimao.wan@anu.edu.au

[†]These authors contributed equally to this work.

ABSTRACT

Crystalline silicon (c-Si) solar cells have been dominating the photovoltaic (PV) market for decades, and c-Si based photoelectrochemical (PEC) cells are regarded as one of the most promising routes for water splitting and renewable production of hydrogen. In this work, we demonstrate a nanoscale tantalum oxide (TaO_x, ~6 nm) as an electron-selective heterocontact, simultaneously providing high quality passivation to the silicon surface and effective transport of electrons to either an external circuit or a water splitting catalyst. The PV application of TaO_x is demonstrated by a proof-of-concept device having a conversion efficiency of 19.1%. In addition, the PEC application is demonstrated by a photon-to-current efficiency (with additional applied bias) of 7.7%. These results represent a 2% and 3.8% absolute enhancement over control devices without a TaO_x interlayer, respectively. The methods presented in this paper are not limited to c-Si based devices, and can be viewed as a more general approach to the interface engineering of optoelectronic and photoelectrochemical applications.

TOC GRAPHICS

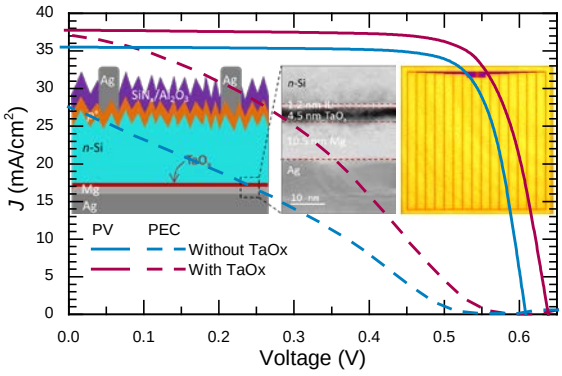

With increasing concerns over rising global energy demand and environmental sustainability, the development of renewable energy technologies is of great importance to the continuation of socio-economic development. There is growing consensus that significant contributions can come from the conversion of solar energy into electricity using photovoltaic (PV) cells[1] and/or into chemical energy using photoelectrochemical (PEC) devices[2]. With a 90% share of global PV market, crystalline silicon (c-Si) is unequivocally the most important photovoltaic technology. Due to its high abundance in the earth crust and industrial maturity, c-Si based systems have also received significant attention for PEC applications[3-7]. Both PV and PEC devices rely on the same central working principle; photo-generated electrons and holes are separately collected at the two opposite terminals of the device. A common method to achieve this function is via doping (i.e., boron-doped p^+ or phosphorus-doped n^+) the near-surface regions of the silicon wafer or thin silicon films deposited on it[8-10].

Another attractive approach to separately collect the two types of charge carriers is to use metal-insulator-semiconductor (MIS) passivated heterocontact structures. A typical MIS heterocontact is composed of a metal layer positioned on the outer surface of an oxide passivated semiconductor. To be able to function as passivated heterocontacts, the oxide interlayers have to fulfil several critical requirements: (i) effective passivation of defects typically present at the silicon surface, (ii) efficient transport of only one carrier type (for example electrons) and effective blocking of the other carrier (for example holes) in their path from the silicon photon absorber to the outer metal terminals, and (iii) simple synthesis method at low thermal budget. Specific to PEC applications, the oxide interlayers also need to be chemically robust to survive in a very harsh aqueous environment for extended operation.

Ultrathin tunnelling silicon dioxide (SiO_2, typically ~ 1.5 nm) is one of the most explored oxides in heterocontacts for both PV[11, 12] and PEC[4, 6, 13, 14] applications, thanks to its reasonable passivation quality and effective transport of carriers (i.e., permits the transport of majority

carriers together with a low recombination of minority carriers)[11, 12] and its stability over a wide range of pH and chemical potentials[15]. However, the highly insulating bulk properties of SiO_2 lead to inhibition of charge transport through the MIS heterocontacts, restricting conduction to tunnelling, or through pinholes. Furthermore, the high quality ultrathin SiO_2 places stringent requirements in film thickness control and process environment purity. Profound efforts have been recently devoted to explore alternatives to SiO_2 as the interlayer to form passivated carrier-selective heterocontacts on c-Si wafers, such as metal salts[16, 17] and oxides[18] and organic polymers[19, 20].

Another group of candidate materials for MIS passivated heterocontacts are the transition metal oxides, some of which possess almost all critical characteristics for carrier selective contacts, including a wide range of work functions, semiconducting properties, and high transparency to sunlight[21]. Research on the incorporation of transition metal oxides into Si-based PV and PEC devices is very recent. High work function oxides such as molybdenum oxide, tungsten oxide, vanadium oxide and cuprous oxide have been explored as hole-selective contacts in silicon solar cells[22-27], whereas nickel oxide and cobalt oxide have been studied as effective photoanodes for water oxidation[28-30]. Remarkably, defective titanium oxide has also been reported to promote hole transport for efficient water oxidation[31, 32]. In contrast, research on transition metal oxides as electron-selective contacts on crystalline silicon is scarce, with titanium oxide and zinc oxide so far the only transition metal oxides reported on Si solar cells[33-35] and strontium titanium oxide as Si photocathodes for water reduction[13].

Although it has not received as much attention yet, tantalum oxide (TaO_x) is a promising material for electron-selective contacts to silicon due to: (i) small conduction band offset[21, 36], which allows electrons from the silicon conduction band to flow through TaO_x, (ii) large valence band offset (~2.9 eV)[21, 36], which provides a barrier to prevent holes in the silicon valence band from flowing to the oxide and further to the metal cathode, and (iii) recently

demonstrated effective passivation of silicon surface defects[37, 38]. In addition, TaO_x possesses high thermal and chemical stability under various pH conditions[39-42], making it a sensible choice for PEC applications. In this work, we report a nanoscale TaO_x film (~6 nm) as a robust passivated electron-selective heterocontact for c-Si based photovoltaics and photoeletrochemical water reduction for the first time, demonstrating significantly improved solar-to-electricity and solar-to-hydrogen conversion efficiencies.

We investigate the optoelectronic properties of TaO_x films synthesised by atomic layer deposition (ALD) and hydrogenated by plasma enhanced chemical vapour deposited (PECVD) silicon nitride (SiN_x), including core-level, valence band, work function, contact resistivity and surface passivation properties. We then demonstrate, for the first time, the application of hydrogenated TaO_x to Si-based PV and PEC devices for the generation of electricity and hydrogen, achieving a solar-to-electricity efficiency of 19.1% and applied bias photon-to-current efficiency of 7.7%, which corresponds to 2% and 3.8% absolute enhancement respectively over control devices without a TaO_x interlayer.

X-ray photoelectron spectroscopy (XPS) was employed to reveal TaO_x electronic properties, including stoichiometry, valence band and work function, which are critical to the transport of electrons. The results are shown in Figure 1. While the Ta 4f spectra shows typical doublet peaks located at 26.5 eV and 28.5 eV for Ta 4f 7/2 and Ta 4f 5/2 respectively[43], the O 1s spectra can be fitted with two Gaussian components with peaks positioned at 530.8 eV and 532 eV, respectively. The small peak located at 532 eV is usually attributed to peroxide O_2^{2-}, although sometimes it can also be due to surface contamination[43]. The component with lower binding energy peaked at 530.8 eV is from Ta-O binding[43]. Notably, the peak positions for both Ta 4f and O 1s are observed to be the same for the TaO_x film before and after SiN_x hydrogenation. However, we can notice a slight reduction in the core level peak areas of O 1s spectra after SiN_x hydrogenation. The extracted TaO_x film stoichiometry based on core level

peak areas is also included in Figure 1(b). The result shows the as deposited TaO_x has an O to Ta atomic fraction of 2.53, and the TaO_x after SiN_x hydrogenation has an O to Ta atomic fraction of 2.44, implying the hydrogenation process makes the TaO_x film slightly more sub-stoichiometric.

Figure 1(c) presents the valence band spectrum of the two TaO_x films, showing no significant difference (< 2% change). Although the TaO_x film after SiN_x hydrogenation is more metallic, no defect band in the band gap can be seen, suggesting negligible amount of filled states at the Fermi level. Further, the XPS secondary electron cut-off result shows that the TaO_x film after SiN_x hydrogenation has a work function of 3.27 eV, approximately 0.3 eV lower than that of as deposited TaO_x. The lower work function can be attributable to the lower cation oxidation state that was revealed by the core level measurements. As proposed in Ref. [44], the lower cation oxidation state would result in lower work function, due to the fact that lower oxidation-state cations are less electronegative than higher oxidation-state cations. The measured work function of the TaO_x films is significantly lower than that of TiO_2 presented in the literature (i.e., ~4.2 eV)[45, 46]. The reduced work function is expected to promote downward band-bending inside the silicon wafer drawing electrons to the surface and consequently improving electron transport.

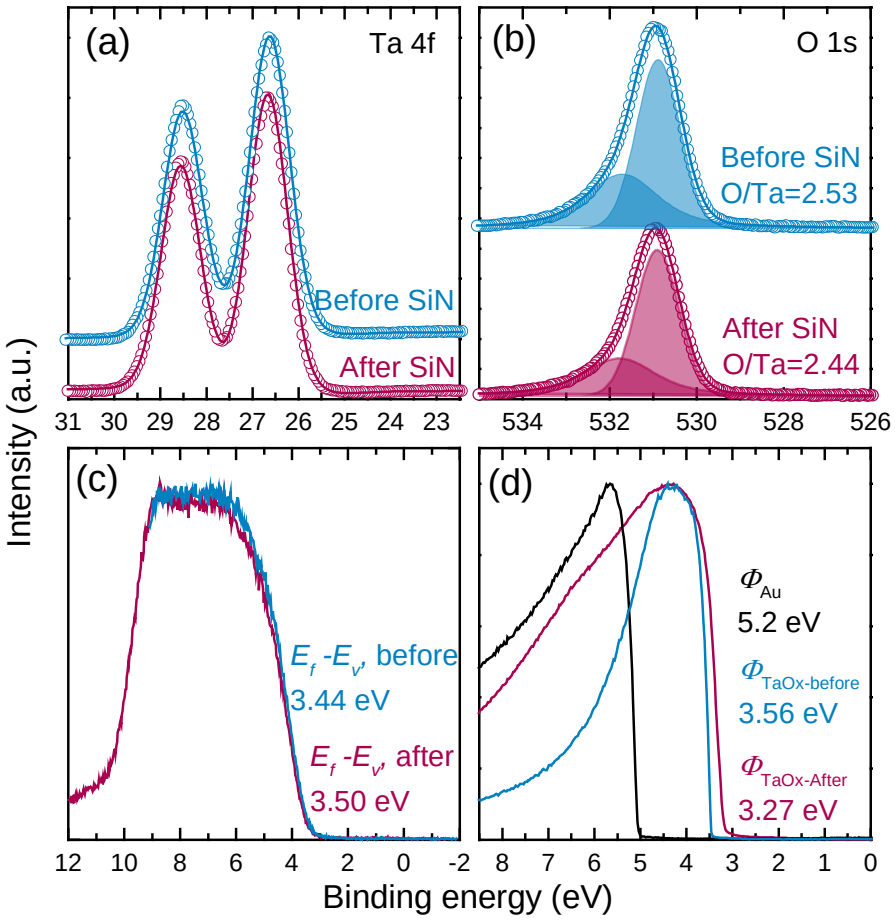

Figure 1: Electronic characterizations of atomic layer deposited TaO_x films before and after hydrogenation. (a) and (b) present the core level spectrum of Ta 4f and O 1s, respectively. (c) shows the valence band spectrum, and (d) shows the secondary electron cut-off spectrum with a gold (Au) reference.

As mentioned above, TaO_x combines a high valence band offset, creating a potential barrier to hole transport; nevertheless, holes can still flow to the interface between TaO_x and Si, unless it is perfectly passivated. Therefore, the carrier selectivity of an *n*-Si/TaO_x hetero-structure needs to be evaluated by characterising not only the contact resistivity ρ_c but also the surface recombination velocity. A highly selective contact is achieved through a simultaneous reduction in recombination and contact resistance. One of the most straightforward techniques to probe the recombination properties of c-Si surfaces is by measuring the effective minority carrier lifetime (τ_{eff}) of symmetrically film-passivated wafers in a contactless fashion[47], as illustrated in Supporting information S1.

Figure 2(a) depicts the quality of surface passivation provided by 6 nm TaO_x films before and after SiN_x hydrogenation by plotting the injection-dependent effective carrier lifetime $\tau_{eff}(\Delta n)$ of *n*-type undiffused c-Si samples. As can be seen, the as-deposited TaO_x film (i.e., before hydrogenation) provides a poor passivation to silicon surfaces, with τ_{eff} of ~30 µs at an excess carrier density $\Delta n = 10^{15}$ cm^{-3}. The level of surface passivation is improved more than one order of magnitude upon a SiN_x hydrogenation treatment, resulting in τ_{eff} as high as ~650 µs at $\Delta n = 10^{15}$ cm^{-3}, corresponding to a recombination current density J_0 of 22.5 fA/cm^2 and an implied V_{OC} of 690 mV. Figure 2(b) shows that the passivation quality of hydrogenated TaO_x films depends strongly on the film thickness; the corresponding injection-dependent lifetime curves are shown in detail as Supporting information Figure S1(b). As the TaO_x thickness increases, τ_{eff} first increases, and then tends to plateau at 8 nm TaO_x. The highest lifetime achieved at $\Delta n = 10^{15}$ cm^{-3} is ~2.7 ms. The substantial enhancement in passivation upon SiN_x hydrogenation is mainly attributable to the hydrogenation of defects at the TaO_x/c-Si interface during the deposition of SiN_x[38].

The contact resistivity ρ_c of TaO_x to *n*-type Si was measured using the method devised by Cox and Strack.[48] The test structure is schematically depicted in Supporting information Figure S2(a). Low work function metal Mg was employed here to further enhance the electron transport, as demonstrated in previous work[49]. Figure 2(c) shows a representative *I*–*V* measurement of TaO_x samples before and after the SiN_x hydrogenation treatment. As can be seen, the sample before SiN_x hydrogenation exhibits severe rectifying behaviour and a high contact resistivity. By contrast, the contact behavior of the TaO_x (~6 nm) film is enhanced dramatically upon SiN_x hydrogenation, resulting in an Ohmic contact to the *n*-type Si substrate. The full series of *I*–*V* measurements are shown in Supporting information Figure S2(b); from that series, the ρ_c for the heterocontact with ~6 nm hydrogenated TaO_x is determined to be ~0.35 $\Omega \cdot cm^2$, which is sufficiently low to function as a full area heterocontact for *n*-type silicon

PV and PEC devices. The good electron transport provided by the hydrogenated TaO_x on *n*-type Si can be attributed to (*i*) a reduced work function, and/or (*ii*) Fermi-level depinning as a consequence of the passivation of interface states between TaO_x and the silicon substrate. The dependence of contact resistivity on TaO_x thickness is depicted in Figure 2(d), exhibiting a slow increase in ρ_c and then a sharp increase when TaO_x is beyond 6 nm. Indeed, when TaO_x thickness exceeds 10 nm, the contact behaves in a rectifying fashion even after the SiN_x hydrogenation. The increasing trend in both τ_{eff} and ρ_c creates a trade-off between surface passivation and contact resistivity provided by the TaO_x film. To resolve this trade-off, we fabricate completed silicon solar cells in order to find the optimum TaO_x film thickness for maximising the carrier selectivity.

Upon quantifying the carrier selectivity of TaO_x, we can now perform a comparison to state-of-the-art electron selective contacts reported in the literature. Table S1 in Supporting Information summarises the performance parameters of the various electron-selective contacts, including work function, contact resistivity, and recombination current density. Compared to the lowest work function materials, such as alkali and alkaline earth metals or salts, TaO_x itself can provide an effective passivation of the silicon surface, with a recombination current density of just J_0 ~22.5 fA/cm^2. In contrast, to achieve low recombination in the case of electron-selective contacts based on alkali or alkaline earth metal salts, it is necessary to insert an additional passivation layer, such as amorphous silicon; without significant compromise in the contact resistivity[50]. The surface passivation quality by TaO_x is slightly better than the recently reported SiO_2/TiO_2 stack which has enabled an efficiency of 22.1% silicon solar cells[51], demonstrating a high potential to achieve high efficiency solar cells by using TaO_x based electron selective heterocontacts. It is notable, however, that in our experiments it has been necessary to hydrogenate the TaO_x/Si interface by depositing a sacrificial layer of SiN_x; it should be possible, however, to perform such hydrogenation by other simpler means, such as

hydrogen plasma treatment[52]. A distinctive feature is that, among all the electron-selective contacts in Table S1, TaO_x exhibits the highest stability against chemical solutions, making it a sensible choice for photoelectrochemical applications.

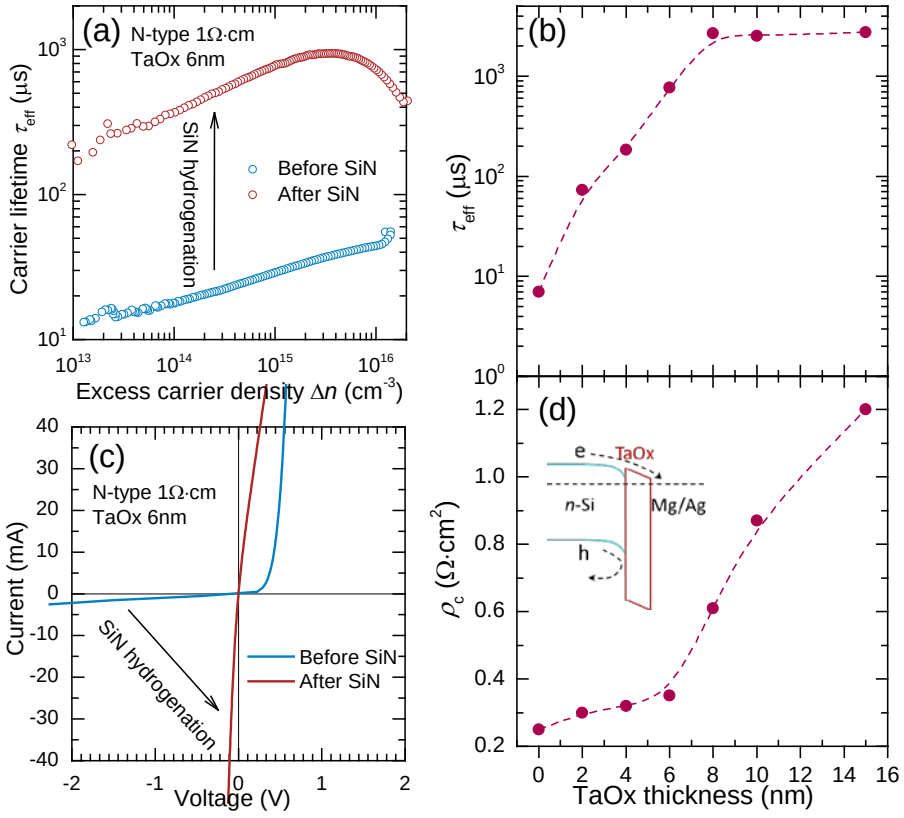

Figure 2: Carrier selectivity characterizations of TaO_x passivated electron heterocontacts to *n*-type c-Si. (a) presents the effective carrier lifetime τ_{eff} versus excess carrier density Δn for c-Si passivated with TaO_x films before and after SiN_x hydrogenation. (b) presents the effect of hydrogenated TaO_x film thickness on τ_{eff}. (c) presents a representative *I*–*V* measurements of TaO_x samples before and after SiN hydrogenation. (d) shows the effect of hydrogenated TaO_x film thickness on the contact resistivity ρ_c. The inset in (d) shows a schematic illustration of band diagram with hydrogenated TaO_x.

The complete silicon solar cells feature full area one dimension TaO_x passivated heterocontacts and are schematically depicted in Figure 3(a). Figure 3(b) presents a cross-sectional transmission electron micrograph of the rear heterocontacts, showing the ~6 nm TaO_x consists of ~1.2 nm interfacial layer and ~4.5 nm TaO_x. The interfacial layer may result from exposure to ambient after deionized water rinse or water precursor during the first few ALD

cycles. A photoluminescence image of the complete solar cells (Figure 3c) employing a 1025 nm short-pass filter shows the cell surfaces had uniform optical, passivating and contact behaviors. Figure 3(d) shows the solar cell power conversion efficiency as a function of TaO_x film thickness (detailed electrical parameters for these cells (V_{OC}, J_{SC}, and *FF*) are presented in Supporting information Figure S3 and Table S2). As can be seen, the efficiency exhibits a strong dependence on TaO_x film thickness, with a maximum at a thickness of 6 nm. As TaO_x film thickness increases, the efficiency first increases primarily due to an increase in surface passivation quality and therefore an enhancement in V_{OC}, and then decreases after 6 nm mainly due to a high contact resistivity imposed by the thicker TaO_x film and therefore a reduction in *FF*. These solar cells trends are consistent with the carrier selectivity results presented in Figure 2.

The illuminated *J–V* curve for the champion cell with 6 nm TaO_x is plotted in Figure 3(e), which also includes the reference cell without a TaO_x film. It can be seen that all cell parameters were improved drastically by inserting the 6 nm thick TaO_x layer, yielding a 19.1% solar-to-electricity conversion efficiency, which is 2% absolute higher than the 17.1% reference cell. Compared to the reference cell with metal directly on silicon, an absolute gain of 29 mV in open-circuit voltage (V_{OC}) was obtained, primarily due to the improved surface passivation provided by the hydrogenated TaO_x film. The suppression of the recombination at rear silicon surfaces also leads to a gain of 2.3 mA/cm^2 in short-circuit current. It is interesting to note that the fill factor is negligibly affected by the insertion of 6 nm TaO_x, despite of a slight increase in contact resistivity. It is worth mentioning that the obtained V_{OC} (638 mV) is significantly lower than the implied V_{OC} from the lifetime sample (~690 mV). One tentative cause for this behavior is the damage to surface passivation during Mg metal evaporation, a behavior that has also been observed for the case of amorphous silicon[49]. A possible solution to mitigate this damage would be the use of other low work function materials such as lithium or magnesium

fluorides[16, 17]. The spectral response plotted in Figure 3(f) shows a similar reflectance but a significant enhancement in the external quantum efficiency (EQE) at long wavelengths (i.e., range from ~900–1200 nm) for the cell with the TaO_x heterocontact, thanks to the passivation of the rear surface by the TaO_x layer. This is consistent with the abovementioned improvements in effective lifetime, voltage and current and provides additional evidence of the enhancements realized from TaO_x passivation.

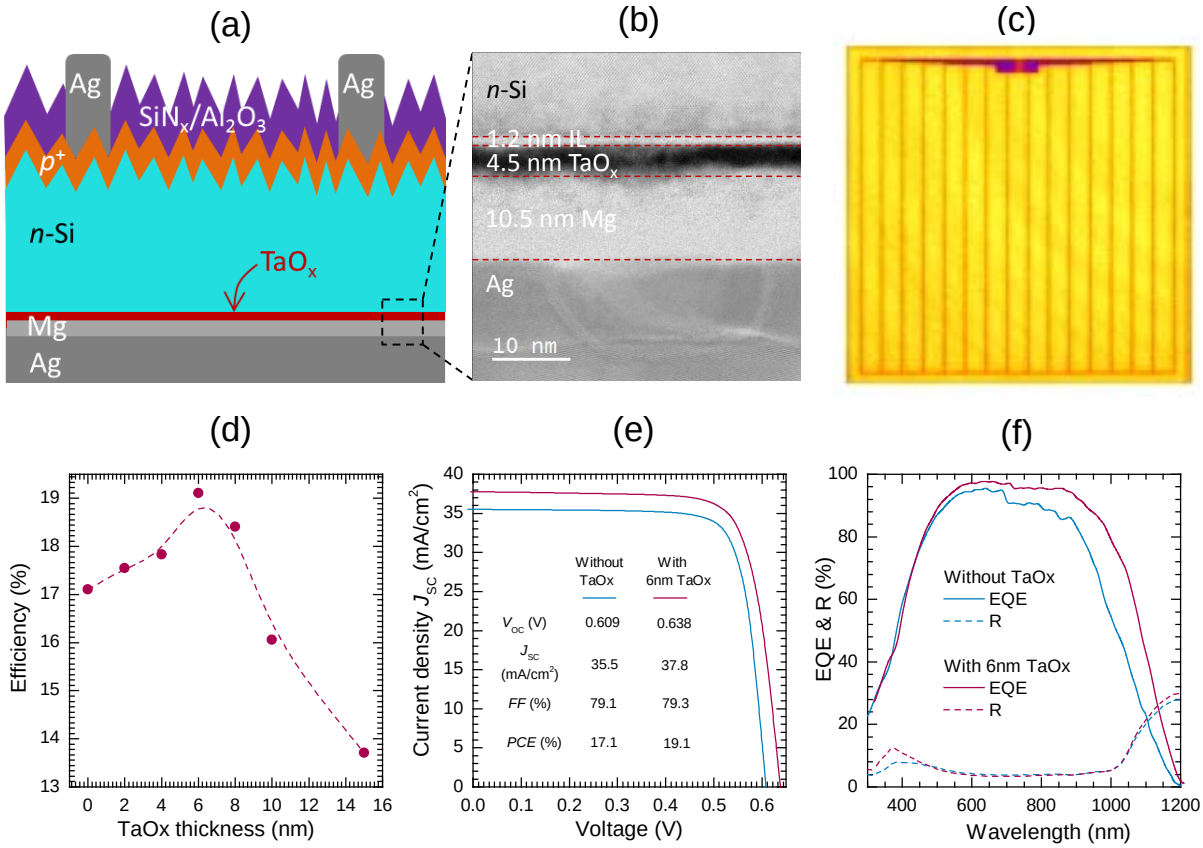

Figure 3: PV device performance with a full-area rear TaO_x passivated electron heterocontact. (a) Schematic cross-section of an *n*-type silicon solar cell featuring a full-area TaO_x/Mg/Ag rear contact. (b)Cross-sectional transmission electron micrograph (TEM) of the rear heterocontacts. (c) Photoluminescence image of the complete solar cell. (d) Dependence of cell efficiency on TaO_x film thickness. (e) Light *J*–*V* curves and electrical parameters of cells with and without a~6 nm TaO_x interlayer. (f) Spectral response (external quantum efficiency and reflectance) of the two cells.

Finally, the concept of electron transport by hydrogenated TaO_x is also demonstrated for photoelectrochemical hydrogen evolution. The electron-selective heterocontact was prepared by replacing the Mg/Ag metal stack, which we found not to be chemically stable, with 5 nm Ti metal and 5 nm Pt catalyst on a ~ 6 nm TaO_x film, to enable stable and efficient hydrogen evolution reactions, as shown in Figure 4(a). Ti metal with its relatively low work function (~ 4.2 eV[53]) assists in reducing the barrier between TaO_x and Pt, improving the photovoltage over a device with Pt only[4]. When the silicon device is illuminated, photogenerated minority carriers (holes in this case) flow towards the illuminated p^+ region at the front surface, whereas the majority carriers (electrons in this case) are transported through the TaO_x interlayer to the outer Ti/Pt catalyst, where the hydrogen evolution reaction takes place.

For comparison, a control PEC device was prepared without a TaO_x film. Figure 4(b) compares the photoelectrochemical performance of these two PEC devices, with and without TaO_x. The control device shows an onset potential of 525 mV for water reduction, whereas the photoelectrode with ~ 6 nm of TaO_x showed a more positive onset potential of 565 mV. The photocurrent density of the device with a TaO_x passivated electrode reaches 37.1 mA/cm^2 at 0V vs RHE, compared to the 27.5 mA/cm^2 obtained for the control electrode without TaO_x. The significant enhancement in both photocurrent and photovoltage is consistent with the improved photovoltaic characteristics shown in Figure 3, and can be attributed to the role of TaO_x in suppressing carrier recombination at the rear surface whilst maintaining efficient electron transport.

To evaluate the improvement in photoelectrochemical performance with TaO_x layer, applied bias photon-to-current efficiency (ABPE) has been calculated using the method reported previously[54]. It is noted that ABPE values derived from three-electrode measurements does not include the losses that might be present at the counter electrode in a two electrode system. ABPE for TaO_x passivated electrode has been measured to reach 7.7% which is almost double

to that of the control electrode without TaO_x interlayer. However, this PEC conversion efficiency is well below the 19.1% achieved by the best photovoltaic device incorporating a TaO_x interlayer, mainly due to lower photovoltage and *FF*. Beyond the thermodynamic energy loss associated with the water reduction electrolyte, this disparity can be largely attributed to an unfavourable energy band alignment in the Ti/TaO_x/Si photocathode, compared to the Mg/TaO_x/Si contact architecture used in the PV devices. The use of Ti instead of Mg, can potentially lead to a higher barrier height for electron transport and therefore cause significant loss in the electron contact resistivity. Nevertheless, these experiments have demonstrated, for the first time, that hydrogentated TaO_x is capable of providing passivation of the silicon surface and, simultaneously, transport efficiently the electrons for PEC water reduction.

As the electrodes used for water splitting must endure a highly corrosive and reducing environment, stability tests have been carried out to evaluate the photoresponse and photostability. As shown in Figure 4(d), the reference electrode exhibited a slight drop in photocurrent with time, while the photoelectrode with TaO_x film showed a highly stable photoresponse. It is known that c-Si is stable in acid environments while it is highly unstable in oxidising conditions. The instability of the control electrode without TaO_x interlayer is likely attributed to the lack of hole blocking effect at the interface, inducing possible self-oxidising conditions. The long-term stability of the TaO_x–based electrode is further confirmed in 1M hydrochloric acid solution for 2 hours of continuous operation (see Supporting information Figure S4).

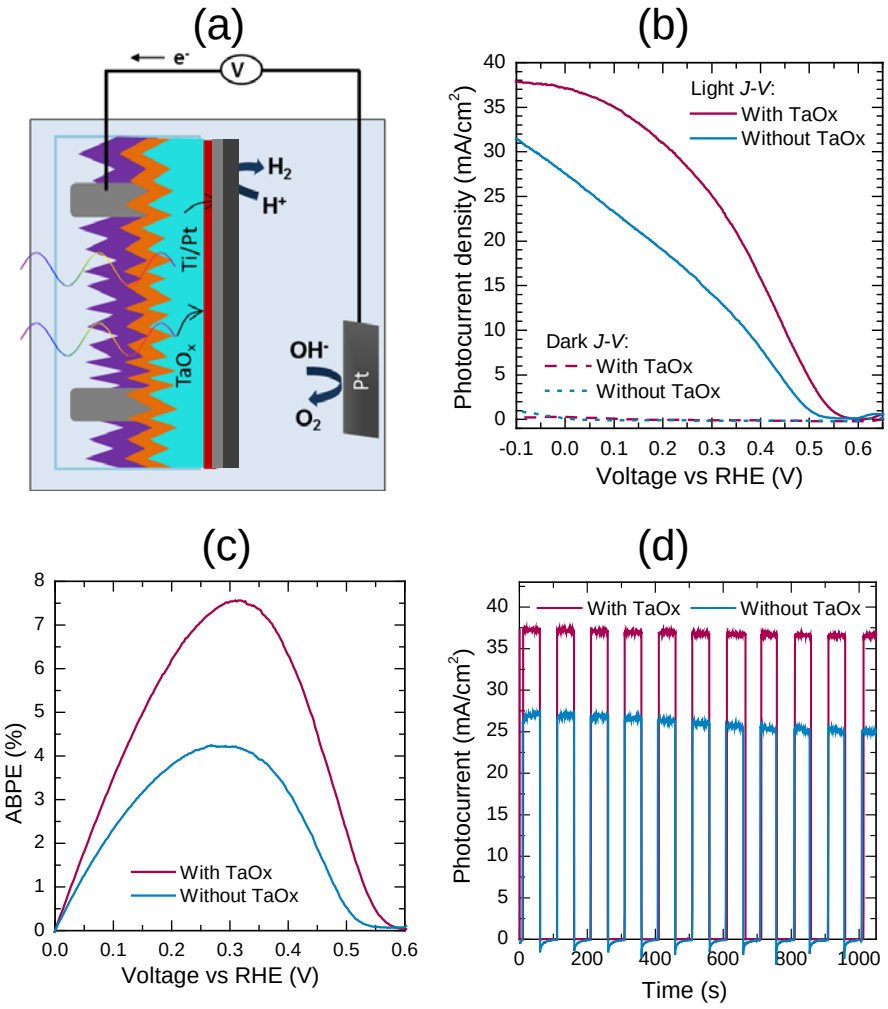

Figure 4: PEC device results with TaO_x passivated electron heterocontacts. (a) illustrates the schematic of an *n*-type silicon photocathode using TaO_x passivated electron heterocontacts. (b) presents the photoelectrochemical current-voltage curves of Si photocathodes with and without ~6 nm TaO_x interlayer. (c) shows applied bias photon-to-current efficiency (ABPE). (d) shows amperometric current-time curves of Si photocathodes at 0V vs the reversible hydrogen electrode (RHE).

Conclusions

We have successfully demonstrated a hydrogenated TaO_x (~6 nm) electron-selective heterocontact that simultaneously provides high quality passivation of the silicon surface (i.e., lifetime ~650 µs) and effective transport of electrons (i.e., contact resistivity ~0.35 $\Omega \cdot cm^2$). The XPS measurements revealed the hydrogenation induced by PECVD SiN_x resulted in reduction in TaO_x stoichiometry and work function, making TaO_x film favourable for electron contacts.

We have achieved a solar-to-electricity efficiency of 19.1% and a solar-to-hydrogen efficiency of 7.7%, which corresponds to a 2% and 3.8% absolute enhancement, respectively, over the control devices without a TaO_x interlayer. These findings related to tantalum oxide are not limited to a silicon-based device platform; more generally, they indicate a generic pathway for interface engineering of optoelectronic and photoelectrochemical applications.

Experimental methods

The TaO_x films were deposited by a thermal ALD reactor (Picosun, R200 Advanced) using Tantalum Ethoxide precursor at 250 °C and had a corresponding growth rate of 0.35 Å/cycle as measured by ex-situ spectroscopic ellipsometry (J.A. Woolam M2000 ellipsometer). The hydrogenation of TaO_x film was realised by capping PECVD SiN_x atop TaO_x and then stripping off the SiN_x layer by 1% hydrofluoric acid, taking advantage of the exceptional chemical stability of TaO_x film under various pH conditions. PECVD SiN_x has been well-known in providing hydrogen to manipulate bulk and interfacial properties of a range of materials such as silicon[55]. The capping SiN_x layer was deposited in a microwave/radio-frequency PECVD reactor (AK400, Roth & Rau)[56], having a thickness of 85 nm and a refractive index of ~1.9 at 632 nm.

Further experimental details are given in the Supporting Information.

ASSOCIATED CONTENT

Supporting Information

Characterization methods including X-ray photoelectron spectroscopy (XPS), carrier lifetime, and contact resistivity, fabrication and characterization details of silicon PV and PEC devices

AUTHOR INFORMATION

Corresponding Author

*yimao.wan@anu.edu.au

Author Contributions

Y.W. supervised the project. Y.W. and S.K. conceived the idea. Y.W. and C.S. carried out the material development, device fabrication, characterization and analysis. Y.W., S.K., and P.R.N. conducted water splitting experiment. J.B. and M.H. assisted with XPS characterization and analysis. D.Y. and J. P. assisted with PV device fabrication and characterization. S.M., H.H.T., C.J., A.J. and A.C. discussed the results. The manuscript was mainly written and revised by Y.W and S.K. All authors commented on the manuscript.

Notes

The authors declare no competing financial interest.

ACKNOWLEDGEMENTS

This work was supported by the Australian Government through the Australian Research Council (ARC). Some facilities at the Australian National Fabrication Facility and Centre for Advanced Microscopy at ANU were used. XPS characterization was performed at the Joint Center for Artificial Photosynthesis, supported through the Office of Science of the US Department of Energy under Award Number DE-SC0004993. A.J., M.H. and J.B. acknowledge funding from the Bay Area Photovoltaics Consortium (BAPVC).

References

(1) Creutzig, F.; Agoston, P.; Goldschmidt, J. C.; Luderer, G.; Nemet, G.; Pietzcker, R. C. The underestimated potential of solar energy to mitigate climate change. *Nature Energy* **2017,** *2*, 17140.
(2) Walter, M. G.; Warren, E. L.; McKone, J. R.; Boettcher, S. W.; Mi, Q.; Santori, E. A.; Lewis, N. S. Solar Water Splitting Cells. *Chemical Reviews* **2010,** *110*, 6446-6473.
(3) Sun, K.; Shen, S.; Liang, Y.; Burrows, P. E.; Mao, S. S.; Wang, D. Enabling Silicon for Solar-Fuel Production. *Chemical Reviews* **2014,** *114*, 8662-8719.
(4) Esposito, D. V.; Levin, I.; Moffat, T. P.; Talin, A. A. H2 evolution at Si-based metal–insulator–semiconductor photoelectrodes enhanced by inversion channel charge collection and H spillover. *Nat Mater* **2013,** *12*, 562-568.
(5) Reece, S. Y.; Hamel, J. A.; Sung, K.; Jarvi, T. D.; Esswein, A. J.; Pijpers, J. J. H.; Nocera, D. G. Wireless Solar Water Splitting Using Silicon-Based Semiconductors and Earth-Abundant Catalysts. *Science* **2011,** *334*, 645-648.
(6) Ji, L.; Hsu, H.-Y.; Li, X.; Huang, K.; Zhang, Y.; Lee, J. C.; Bard, A. J.; Yu, E. T. Localized dielectric breakdown and antireflection coating in metal-oxide-semiconductor photoelectrodes. *Nat Mater* **2017,** *16*, 127-131.

(7) Zhou, X.; Liu, R.; Sun, K.; Papadantonakis, K. M.; Brunschwig, B. S.; Lewis, N. S. 570 mV photovoltage, stabilized n-Si/CoOx heterojunction photoanodes fabricated using atomic layer deposition. *Energy & Environmental Science* **2016,** *9*, 892-897.
(8) Zhao, J. Recent advances of high-efficiency single crystalline silicon solar cells in processing technologies and substrate materials. *Solar Energy Materials and Solar Cells* **2004,** *82*, 53-64.
(9) Glunz, S.; Feldmann, F.; Richter, A.; Bivour, M.; Reichel, C.; Steinkemper, H.; Benick, J.; Hermle, M. In *The irresistible charm of a simple current flow pattern - approaching 25% with a solar cell featuring a full-area back contact*, 31st European Photovoltaic Solar Energy Conference and Exhibition, Hamburg, Germany, September, 2015; Hamburg, Germany.
(10) Masuko, K.; Shigematsu, M.; Hashiguchi, T.; Fujishima, D.; Kai, M.; Yoshimura, N.; Yamaguchi, T.; Ichihashi, Y.; Mishima, T.; Matsubara, N., et al. Achievement of More Than 25% Conversion Efficiency With Crystalline Silicon Heterojunction Solar Cell. *Photovoltaics, IEEE Journal of* **2014,** *4*, 1433-1435.
(11) Godfrey, R. B.; Green, M. A. 655 mV open‐circuit voltage, 17.6% efficient silicon MIS solar cells. *Applied Physics Letters* **1979,** *34*, 790-793.
(12) Green, M. A.; Blakers, A. W. Advantages of metal-insulator-semiconductor structures for silicon solar cells. *Solar Cells* **1983,** *8*, 3-16.
(13) Ji, L.; McDaniel, M. D.; Wang, S.; Posadas, A. B.; Li, X.; Huang, H.; Lee, J. C.; Demkov, A. A.; Bard, A. J.; Ekerdt, J. G., et al. A silicon-based photocathode for water reduction with an epitaxial SrTiO3 protection layer and a nanostructured catalyst. *Nat Nano* **2015,** *10*, 84-90.
(14) Hill, J. C.; Landers, A. T.; Switzer, J. A. An electrodeposited inhomogeneous metal-insulator-semiconductor junction for efficient photoelectrochemical water oxidation. *Nat Mater* **2015,** *14*, 1150-1155.
(15) Pourbaix, M., *Atlas of Electrochemical Equilibria in Aqueous Solutions*. 2nd edn ed.; National Association of Corrosion Engineers: Science, 1974.
(16) Bullock, J.; Zheng, P.; Jeangros, Q.; Tosun, M.; Hettick, M.; Sutter-Fella, C. M.; Wan, Y.; Allen, T.; Yan, D.; Macdonald, D., et al. Lithium Fluoride Based Electron Contacts for High Efficiency n-Type Crystalline Silicon Solar Cells. *Advanced Energy Materials* **2016,** *6*, 1600241.
(17) Wan, Y.; Samundsett, C.; Bullock, J.; Allen, T.; Hettick, M.; Yan, D.; Zheng, P.; Zhang, X.; Cui, J.; McKeon, J., et al. Magnesium Fluoride Electron-Selective Contacts for Crystalline Silicon Solar Cells. *ACS Applied Materials & Interfaces* **2016,** *8*, 14671-14677.
(18) Wan, Y.; Samundsett, C.; Bullock, J.; Hettick, M.; Allen, T.; Yan, D.; Peng, J.; Wu, Y.; Cui, J.; Javey, A., et al. Conductive and Stable Magnesium Oxide Electron-Selective Contacts for Efficient Silicon Solar Cells. *Advanced Energy Materials* **2017,** *7*, 1601863-n/a.
(19) Schmidt, J.; Titova, V.; Zielke, D. Organic-silicon heterojunction solar cells: Open-circuit voltage potential and stability. *Applied Physics Letters* **2013,** *103*, 183901.
(20) Zhang, Y.; Zu, F.; Lee, S. T.; Liao, L.; Zhao, N.; Sun, B. Heterojunction with organic thin layers on silicon for record efficiency hybrid solar cells. *Advanced Energy Materials* **2014,** *4*, 1300923.
(21) Greiner, M. T.; Helander, M. G.; Tang, W.-M.; Wang, Z.-B.; Qiu, J.; Lu, Z.-H. Universal energy-level alignment of molecules on metal oxides. *Nat Mater* **2012,** *11*, 76-81.
(22) Battaglia, C.; de Nicolás, S. M.; De Wolf, S.; Yin, X.; Zheng, M.; Ballif, C.; Javey, A. Silicon heterojunction solar cell with passivated hole selective MoOx contact. *Applied Physics Letters* **2014,** *104*, 113902.
(23) Battaglia, C.; Yin, X.; Zheng, M.; Sharp, I. D.; Chen, T.; McDonnell, S.; Azcatl, A.; Carraro, C.; Ma, B.; Maboudian, R. Hole selective MoO x contact for silicon solar cells. *Nano letters* **2014,** *14*, 967-971.
(24) Bivour, M.; Temmler, J.; Steinkemper, H.; Hermle, M. Molybdenum and tungsten oxide: High work function wide band gap contact materials for hole selective contacts of silicon solar cells. *Solar Energy Materials and Solar Cells* **2015,** *142*, 34-41.
(25) Bullock, J.; Cuevas, A.; Allen, T.; Battaglia, C. Molybdenum oxide MoOx: A versatile hole contact for silicon solar cells. *Applied Physics Letters* **2014,** *105*, 232109.
(26) Geissbühler, J.; Werner, J.; Martin de Nicolas, S.; Barraud, L.; Hessler-Wyser, A.; Despeisse, M.; Nicolay, S.; Tomasi, A.; Niesen, B.; De Wolf, S., et al. 22.5% efficient silicon heterojunction solar cell with molybdenum oxide hole collector. *Applied Physics Letters* **2015,** *107*, 081601.
(27) Zhang, X.; Wan, Y.; Bullock, J.; Allen, T.; Cuevas, A. Low resistance Ohmic contact to p-type crystalline silicon via nitrogen-doped copper oxide films. *Applied Physics Letters* **2016,** *109*, 052102.
(28) Chen, L.; Yang, J.; Klaus, S.; Lee, L. J.; Woods-Robinson, R.; Ma, J.; Lum, Y.; Cooper, J. K.; Toma, F. M.; Wang, L.-W., et al. p-Type Transparent Conducting Oxide/n-Type Semiconductor Heterojunctions for Efficient and Stable Solar Water Oxidation. *Journal of the American Chemical Society* **2015,** *137*, 9595-9603.
(29) Kenney, M. J.; Gong, M.; Li, Y.; Wu, J. Z.; Feng, J.; Lanza, M.; Dai, H. High-Performance Silicon Photoanodes Passivated with Ultrathin Nickel Films for Water Oxidation. *Science* **2013,** *342*, 836-840.

(30) Sun, K.; Park, N.; Sun, Z.; Zhou, J.; Wang, J.; Pang, X.; Shen, S.; Noh, S. Y.; Jing, Y.; Jin, S., et al. Nickel oxide functionalized silicon for efficient photo-oxidation of water. *Energy & Environmental Science* **2012,** *5*, 7872-7877.
(31) Chen, Y. W.; Prange, J. D.; Dühnen, S.; Park, Y.; Gunji, M.; Chidsey, C. E. D.; McIntyre, P. C. Atomic layer-deposited tunnel oxide stabilizes silicon photoanodes for water oxidation. *Nat Mater* **2011,** *10*, 539-544.
(32) Hu, S.; Shaner, M. R.; Beardslee, J. A.; Lichterman, M.; Brunschwig, B. S.; Lewis, N. S. Amorphous TiO2 coatings stabilize Si, GaAs, and GaP photoanodes for efficient water oxidation. *Science* **2014,** *344*, 1005-1009.
(33) Allen, T. G.; Bullock, J.; Jeangros, Q.; Samundsett, C.; Wan, Y.; Cui, J.; Hessler-Wyser, A.; De Wolf, S.; Javey, A.; Cuevas, A. A Low Resistance Calcium/Reduced Titania Passivated Contact for High Efficiency Crystalline Silicon Solar Cells. *Advanced Energy Materials* **2017,** *7*, 1602606.
(34) Avasthi, S.; McClain, W. E.; Man, G.; Kahn, A.; Schwartz, J.; Sturm, J. C. Hole-blocking titanium-oxide/silicon heterojunction and its application to photovoltaics. *Applied Physics Letters* **2013,** *102*, 203901.
(35) Wang, F.; Zhao, S.; Liu, B.; Li, Y.; Ren, Q.; Du, R.; Wang, N.; Wei, C.; Chen, X.; Wang, G., et al. Silicon solar cells with bifacial metal oxides carrier selective layers. *Nano Energy* **2017,** *39*, 437-443.
(36) Robertson, J.; Chen, C. W. Schottky barrier heights of tantalum oxide, barium strontium titanate, lead titanate, and strontium bismuth tantalate. *Applied Physics Letters* **1999,** *74*, 1168-1170.
(37) Wan, Y.; Bullock, J.; Cuevas, A. Passivation of c-Si surfaces by ALD tantalum oxide capped with PECVD silicon nitride. *Solar Energy Materials and Solar Cells* **2015,** *142*, 42-46.
(38) Wan, Y.; Bullock, J.; Cuevas, A. Tantalum oxide/silicon nitride: A negatively charged surface passivation stack for silicon solar cells. *Applied Physics Letters* **2015,** *106*, 201601.
(39) Anderson, M. D.; Aitchison, B.; Johnson, D. C. Corrosion Resistance of Atomic Layer Deposition-Generated Amorphous Thin Films. *ACS applied materials & interfaces* **2016,** *8*, 30644-30648.
(40) Li, C.; Wang, T.; Luo, Z.; Zhang, D.; Gong, J. Transparent ALD-grown Ta2O5 protective layer for highly stable ZnO photoelectrode in solar water splitting. *Chemical communications* **2015,** *51*, 7290-7293.
(41) Chen, S.; Wang, L.-W. Thermodynamic Oxidation and Reduction Potentials of Photocatalytic Semiconductors in Aqueous Solution. *Chemistry of Materials* **2012,** *24*, 3659-3666.
(42) Hu, S.; Lewis, N. S.; Ager, J. W.; Yang, J.; McKone, J. R.; Strandwitz, N. C. Thin-Film Materials for the Protection of Semiconducting Photoelectrodes in Solar-Fuel Generators. *The Journal of Physical Chemistry C* **2015,** *119*, 24201-24228.
(43) Atanassova, E.; Spassov, D. X-ray photoelectron spectroscopy of thermal thin Ta2O5 films on Si. *Applied Surface Science* **1998,** *135*, 71-82.
(44) Greiner, M. T.; Chai, L.; Helander, M. G.; Tang, W.-M.; Lu, Z.-H. Transition Metal Oxide Work Functions: The Influence of Cation Oxidation State and Oxygen Vacancies. *Advanced Functional Materials* **2012,** *22*, 4557-4568.
(45) Imanishi, A.; Tsuji, E.; Nakato, Y. Dependence of the Work Function of TiO2 (Rutile) on Crystal Faces, Studied by a Scanning Auger Microprobe. *The Journal of Physical Chemistry C* **2007,** *111*, 2128-2132.
(46) Peng, J.; Duong, T.; Zhou, X.; Shen, H.; Wu, Y.; Mulmudi, H. K.; Wan, Y.; Zhong, D.; Li, J.; Tsuzuki, T., et al. Efficient Indium-Doped TiOx Electron Transport Layers for High-Performance Perovskite Solar Cells and Perovskite-Silicon Tandems. *Advanced Energy Materials* **2017,** *7*, 1601768-n/a.
(47) Sinton, R. A.; Cuevas, A. Contactless determination of current--voltage characteristics and minority-carrier lifetimes in semiconductors from quasi-steady-state photoconductance data. *Applied Physics Letters* **1996,** *69*, 2510-2512.
(48) Cox, R. H.; Strack, H. Ohmic contacts for GaAs devices. *Solid-State Electronics* **1967,** *10*, 1213-1218.
(49) Wan, Y.; Samundsett, C.; Yan, D.; Allen, T.; Peng, J.; Cui, J.; Zhang, X.; Bullock, J.; Cuevas, A. A magnesium/amorphous silicon passivating contact for n-type crystalline silicon solar cells. *Applied Physics Letters* **2016,** *109*, 113901.
(50) Bullock, J.; Hettick, M.; Geissbühler, J.; Ong, A. J.; Allen, T.; Sutter-Fella, C. M.; Chen, T.; Ota, H.; Schaler, E. W.; Wolf, S. D., et al. Efficient silicon solar cells with dopant-free asymmetric heterocontacts. *Nature Energy* **2016,** *1*.
(51) Yang, X.; Weber, K.; Hameiri, Z.; De Wolf, S. Industrially feasible, dopant-free, carrier-selective contacts for high-efficiency silicon solar cells. *Progress in Photovoltaics: Research and Applications* **2017,** *25*, 896-904.
(52) Descoeudres, A.; Barraud, L.; De Wolf, S.; Strahm, B.; Lachenal, D.; Guerin, C.; Holman, Z. C.; Zicarelli, F.; Demaurex, B.; Seif, J., et al. Improved amorphous/crystalline silicon interface passivation by hydrogen plasma treatment. *Applied Physics Letters* **2011,** *99*, 123506-3.
(53) Sze, S. M.; Ng, K. K., *Physics of semiconductor devices*. John wiley & sons: Hoboken, NJ, USA, 2006.
(54) Boettcher, S. W.; Warren, E. L.; Putnam, M. C.; Santori, E. A.; Turner-Evans, D.; Kelzenberg, M. D.; Walter, M. G.; McKone, J. R.; Brunschwig, B. S.; Atwater, H. A., et al. Photoelectrochemical Hydrogen Evolution Using Si Microwire Arrays. *Journal of the American Chemical Society* **2011,** *133*, 1216-1219.

(55) Aberle, A. G. Overview on SiN surface passivation of crystalline silicon solar cells. *Solar Energy Materials and Solar Cells* **2001,** *65*, 239-248.
(56) Wan, Y.; McIntosh, K. R.; Thomson, A. F. Characterisation and optimisation of PECVD SiNx as an antireflection coating and passivation layer for silicon solar cells. *AIP ADVANCES* **2013,** *3*, 032113.